arXiv:1409.2827v1 [physics.optics] 9 Sep 2014

Laser-Writing in Silicon for 3D Information Processing

O. Tokel,[1,2] A. Turnalı,[1,2] I. Pavlov,[1,2] S. Tozburun,[3,4] I. Akca,[3,4] and F. Ö. Ilday[1,2,a)]

[1)] *Department of Electrical and Electronics Engineering, Bilkent University, 06800, Ankara, Turkey*

[2)] *Department of Physics, Bilkent University, 06800, Ankara, Turkey*

[3)] *Harvard Medical School, Boston, Massachusetts, 02115 USA*

[4)] *Wellman Center for Photomedicine, Massachusetts General Hospital, Boston, Massachusetts, 02114, USA*

(Dated: 10 September 2014)

Micromachining of silicon with lasers is being investigated since the 1970s. So far generating subsurface modifications buried inside the bulk of the silicon without damaging the surface has not resulted in success. Here, we report a method for photo-inducing buried structures in doped silicon wafers with pulsed infrared lasers without modifying the wafer surface. We demonstrate large aspect-ratio, continuous multilevel subsurface structures, with lengths on the millimetre scale, while having sub-micron widths. We further demonstrate spatial information encoding capabilities embedded in subsurface silicon barcodes based on an optical coherence tomography (OCT) readout. The demonstrated silicon processing technology can be used for the realization of multilayered silicon chips, optofluidics and on-chip quantum optics experiments.

Keywords: Silicon, Subsurface, Nonlinear, Laser, Processing, 3D

[a)] http://ufolab.bilkent.edu.tr/UFOLab.

Functional elements that can modulate, process, guide or detect light are highly desirable in silicon photonics because integrating optical elements on a monolithic electronics chip extends the capabilities of the well-established CMOS technology[1]. Successful integration of these photonics and data transfer elements with conventional integrated circuits is proposed to lead to new generations of microprocessors[2,3]. Silicon-on-insulator (SOI) platform is the main architectural approach for the fabrication of functional elements in silicon photonics applications[4]. Notably, silicon lasers have been demonstrated based on this platform[5,6]. Active and passive optical elements are integrated into electronic chips with fabrication techniques such as lithography and etching. These techniques fabricate the optical elements in the top thin layer of SOI platform. In spite of its remarkable successes, this approach does not make use of the bulk of the silicon for positioning functional elements. New fabrication approaches taking advantage of the real estate under the silicon surface can pave the way for creating multi-layered and multi-functional electronic devices with electronic-photonic integration.

Surface lithography on silicon with laser diffraction and interference has been demonstrated[7,8]. More direct laser-writing methods which pattern the surface of silicon have been developed to create microcolumn arrays[9] and surface ripples[10]. Fabrication of controlled patterns on silicon allowed the creation of black-silicon[11,12] with improved spectral sensitivity for applications in solar cells, as well as curious effects such as superwicking silicon[13], on which water flows against the gravity. Recently, laser printing of silicon nanoparticles with precisely controlled sizes has been demonstrated with femtosecond lasers[14]. These techniques are common in the sense that all relevant photo-physical processes take place on the wafer surface. Unfortunately, translation of these methods to a subsurface silicon lithography method has not been possible so far.

Laser microfabrication of transparent materials is an enabling technology for fabricating three-dimensional structures[15]. It has been extensively applied to glasses and polymers in the past decade[16]. Depending on the time scale, intensity and pulse energy of the laser, photons can nonlinearly transfer their energy to the medium to create a seed electron population (i.e., multi-photon ionization) and also to phonons to induce a threshold-based nonlinear breakdown (i.e., avalanche ionization)[17,18]. The exploitation of these nonlinear processes have allowed the fabrication of various optical elements, including waveguides[19], interconnects[20], and resonators[21] buried in the bulk of transparent materials such as fused silica and lithium

niobate crystal. We propose and demonstrate that it is possible to translate this approach to silicon, partly because lasers operating at the corresponding energy regime for silicon are becoming available[22].

An important component in extending the planar topologies and developing 3D functional elements inside silicon would be creating continuous structures inside the wafer. Analogous structures laser scribed in glass have been used as construction elements in diverse applications including a Bragg grating[23], a 3D Mach-Zender interferometer in a microfluidic chip[24], and recently in integrated quantum optical circuit experiments[25,26]. Hybrid laser fabrication methods have been developed to create 3D silicon photonic crystals in a woodpile architecture[27]. From the perspective of nano-photonics, integrating optical interconnects for chip-to-chip and intrachip communication is a holy-grail for the CMOS technology[28]. Notably, the research on photonic integrated circuits is mainly focused on 2D planar architectures. Unconventional, 3D fabrication methods in silicon, analogous to the Through-Silicon-Via technology are needed to overcome the fabrication barrier in the z-direction and for enhanced integration of optical interconnects into electronic chips[29].

Here we built upon the first two-photon subsurface laser processing method of silicon[30], and now create a plethora of subsurface structures buried in silicon without inducing any surface modifications. This technology relies on a direct laser-writing method, which does not require any conventional lithography. Moreover, the structures are continuous and ordered, and are fabricated with very large aspect ratios. These subsurface structures can be created in various geometries, such as a mesh or spiral pattern, or any other complex pattern allowed by the motion of a three-axis translational stage. To demonstrate the 3D information processing capability, we used an optical coherence tomography (OCT) based readout and demonstrated a simple 3D barcode system for decoding of information laser encoded in the wafer.

The advantage of the silicon industry has always been being able to cram more complexity in the wafer. We believe this laser-writing technology will contribute to the existing silicon fabrication capabilities and will find applications in diverse fields, such as silicon photonics, optofluidics and potentially in on-chip quantum photonics experiments. Further, silicon is very rich with nonlinear effects, and one can envisage the use of these effects in future laser-writing experiments and expand the building blocks for creating a fabrication toolbox of deep silicon engineering.

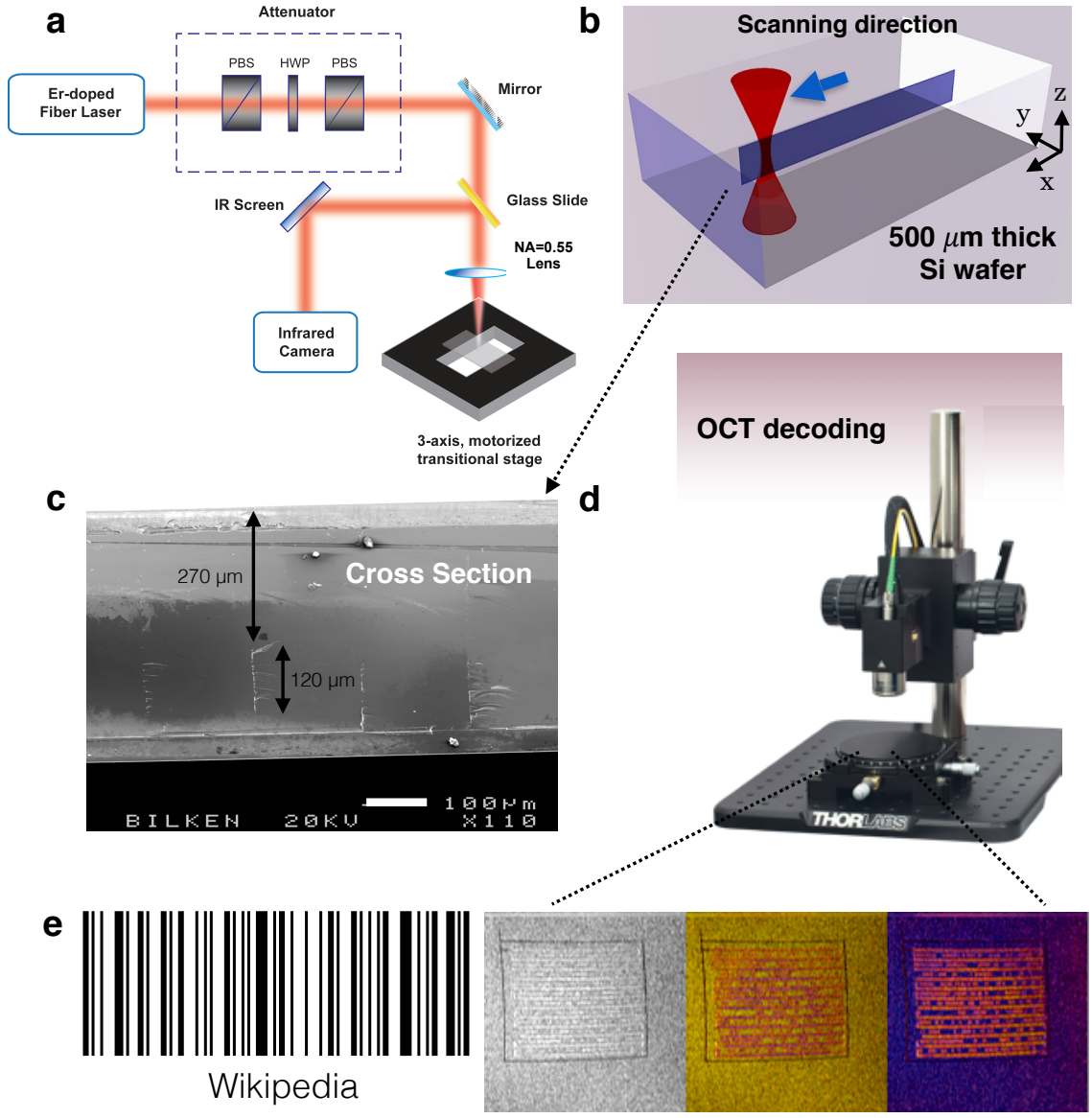

FIG. 1. **Fabrication inside silicon, encoding information and decoding with OCT.** (**a**) Schematic of the experimental setup for direct laser-writing in silicon. PBS: polarizing beam splitter. HWP: half wave plate, NA: numerical Aperture, COL: collimator, (**b**) Tightly focused laser beam creating the high-aspect ratio structures within the wafer. (**c**) Scanning Electron Microscopy image of the cross section of the wafer. The cross section corresponds to the dotted rectangle shown in (**b**). The length of the laser written structures are ≈ 100 μm, their width is sub-micron and their length in the scanning direction is only limited by the wafer size. (**d**) Optical Coherence Tomography (OCT) used for the barcode system. Intensity, local retardation and phase difference retardation modalities can be used. (**e**) Laser encoded information inside silicon samples and OCT readouts of the barcode system. The image on the left shows 'Wikipedia' encoded in a common 1D barcode. The image on the right shows OCT readouts of a barcode.

Results

Fabrication technique.

3D integrated chip technology is an emerging field with the potential to transcend the scaling issues which Moore's law is bound to experience in the coming decade[31]. Variants of 3D packaging methods already allow a smaller form-factor and help overcome some of the power density, signal transmission and speed limitations of densely packaged integrated circuits. The current methods simply rely on stacking dies on top of each other and connecting them with wire-bonding in the 3rd dimension[32]. Aside from improvements in power and transmission, 3D interconnects can be formed among elements located at different chip layers, which can add an abstract layer of design structure in network topologies[33].

The significant potential of photonic-electronic integration can not be fulfilled without alternative fabrication methods in 3D topologies. In this paper, a new direct-laser technique for sub-wafer silicon engineering is developed. The technique allows the generation, positioning and control of continuous structures with the help of tighty-focused laser pulses. Tightly focused femtosecond lasers have already been used for nano-patterning on sample surfaces[34]. Here, the focusing allows nano-patterning inside the wafer. Similar methods have been applied to glasses to induce refractive index changes[16]. However, these methods do not benefit from the doping of semiconductors, which can tailor the absorption of laser light within the material and help engineer the photo-induced interaction[35]. Another advantage of the method is that it is simple, rapid and can be applicable to different semiconductors.

We incorporated a home-made high pulse-energy, all-fibre-integrated master-oscillator power amplifier (MOPA) system to our processing station. The system can produce 5 ns, 10 W pulses at 100 kHz at 1.550 μm. To our knowledge this is the highest-pulse energy reported at this wavelength for single-mode operation and the details of the laser system are reported elsewhere[22]. The laser light collimated from the MOPA system is directed to the material processing station. Our experimental setup is illustrated in Figure 1a. In the experiments we can control the pulse energy with a half-wave plate while the polarization after polarizing beam splitter (PBS) is linear and in the plane of the sample surface. A second half-wave plate before the lens can control the polarization to check the effect of crystal orientation with respect to the polarization during the scans. The laser is operated at 150 kHz and 1.2 W corresponding to 8 μJ pulse energies just before the sample. The laser light from the fibre is tightly focused (f=4.5 mm, NA=0.55) onto a silicon sample which is doped with

boron (150 Ω.cm). Experimentally, we found that one of the most critical elements is precise sample alignment with respect to the laser. This is accomplished by using interference from multiple back-reflections from the 500 μm thick sample's front and back surfaces, which is monitored with an IR sensitive camera. Slight misalignment of the lens can also adversely effect laser-scribing quality. We should also note that the samples must be cleaned with Piranha solution before operation (see Methods).

Two-photon absorption (TPA) at 1.550 μm where silicon is transparent is used to control the location and morphology of the structures[35]. The laser is first focused on the wafer surface where precise alignment is done at low energies, and then sample is translated 300 μm in the laser propagation direction. The sample is raster-scanned with a computer-controlled motorized stage in a plane perpendicular to the laser propagation direction and at speeds in the 0.2-1.0 mm/sec range. The raster-scan is done by alternating the scan direction for each consecutive line. Each linear modification is separated by 50-100 μm from the next line to minimize any possible cross-talk between structures during the writing process. We observed continuous subsurface structures formed along the transversed path of the focal spot of the laser (Figure 1b). A representative SEM image of these buried periodic structures is shown in Figure 1c. It is notable that these structures are not formed as lines, as one would expect at first, but are created in a wall-like geometry. Further, these structures are created continuously, and limited in extent only by the size of the wafer. This is notable, considering the difficulties encountered in creating continuous nano-patterning experiments with various focused-laser methods[36]. We have also constructed a home-made infrared microscope to be able to study the laser-written patterns, as there is no conventional in-situ method that allows studying inside silicon wafers (see Methods).

The direct-write nature of the 3D silicon printing allows one to create a multitude of geometries. This rich space can be used to encode information inside silicon for example to create a barcode. The readout can be accomplished with an OCT system, operating at 980 nm, where silicon is still transparent (Figure 1d). To demonstrate this concept, we have encoded and decoded various planar barcodes imprinted in silicon, such as a common barcode (UPC, code 128). Two examples are shown in Figure 1e, where three-modalities of the OCT are used to decode the matrix pattern. This simple method can be easily extended to create more complicated patterns or even multi-layered images in silicon.

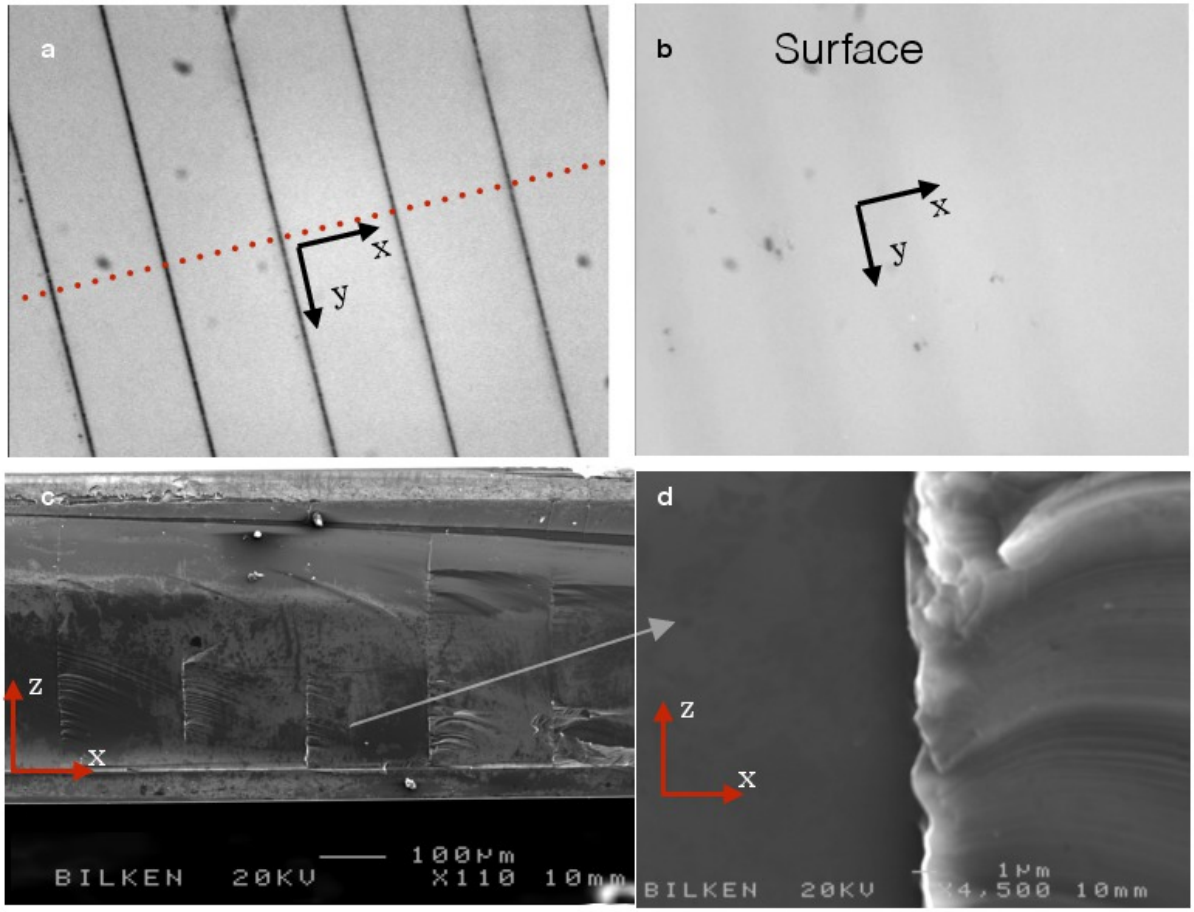

FIG. 2. **Microscope images of the silicon sample after laser processing.** The laser propagates along the z-axis in all images. (***a***-***b***) A modified Olympus microscope is used in the transmission mode to image the bulk of the silicon. Since Si is transparent to the IR tail of the halogen lamp used, and the EMCCD camera is sensitive to IR at this wavelength range we can acquire subsurface images. (***a***) Image acquired by focusing the objective to the centre of the silicon wafer. The plane passing through the red-dotted line and the z-axis is used in the cross-sectional SEM studies. (***b***) Image showing the surface of the wafer, indicating that the surface is clean after subsurface processing. Faint shadows of the buried structures are also visible. Scanning electron microscope (SEM) images of the cross-section of the sample. (***c***-***d***) The sub-surface lines are 200 μm separated. The laser enters from the top of the image and propagates to the bottom, along the z-axis. (***c***) A general view of the structures formed in the x-axis shown along the dotted line in Figure 2a. (***d***) A zoomed image of a single wall-like structure. The modification continues approximately 180 μm along the laser propagation direction, without significantly changing its width. During mechanical sample cutting for SEM sample preparation, stress induces wavy structures which are visible on the right half of image.

Physical characteristics of subsurface structures.

We did not observe any photo-induced modifications on either side of the wafer surface after laser processing. To confirm this, laser-written samples were studied with reflection microscopy operating at optical wavelengths where silicon is opaque, and also with infrared microscopy. Fig 2b shows the laser entrance surface of the sample after writing. Subsurface structures manifest themselves as faint shadows when the image plane is located on the wafer surface (see Supplementary Movie 1). The image plane is shifted to the middle of the wafer to focus on the laser-written structures and a representative image of the laser-scribed structures in shown Figure 2a. The structures continue over 3 mm along the laser scanning direction and are not constrained in this degree-of-freedom by any fundamental physical limitation. This long-range continuity is quite promising from a fabrication point-of-view. Moreover, in our experiments we did not observe any asymmetry resulting from the scanning-direction with respect to the crystal axis. This is in accordance with the fact that Si is a centrosymmetric material, and therefore asymmetries that has been shown to exist in non-centrosymmetrical material laser processing from directional heat accumulation are not expected in Si[37].

The direct laser-writing technique allows us to routinely create sub-surface nanostructures with aspect ratios > 100. Such 3D nanostructures can lead to the formation of previously unattainable morphologies when used in conjunction with pattern transfer techniques including etching, molding and deposition. To study the morphology and dimensions of the buried structures, we diced the samples through the cross-sectional plane shown in Figure 2a. The samples are then evaluated with a scanning electron microscope (SEM) at different magnifications. A representative cross-section is shown in Figure 2c along with a close-up image of one of these lines in Figure 2d. A particularly striking feature of these nano-lines is that the width of the lines remains at sub-micron scale for 100 μm in the laser propagation direction. This is in contrast to conventional nonlinear laser lithography of transparent materials, in which the laser is focused to a spot and the modifications are one-dimensional. The observed behaviour is analogous to filamentation effect seen in femtosecond laser material processing in transparent media[38].

To further elucidate the behaviour of the formation of the nano-walls, we studied the effect of laser polarization on their creation. Figure 3a shows a buried mesh pattern in silicon, with a 50-μm inter-wall distance. The laser polarization was vertical, along one of the crystal axes. The experiment is repeated with the polarization rotated by 90 degrees and is shown

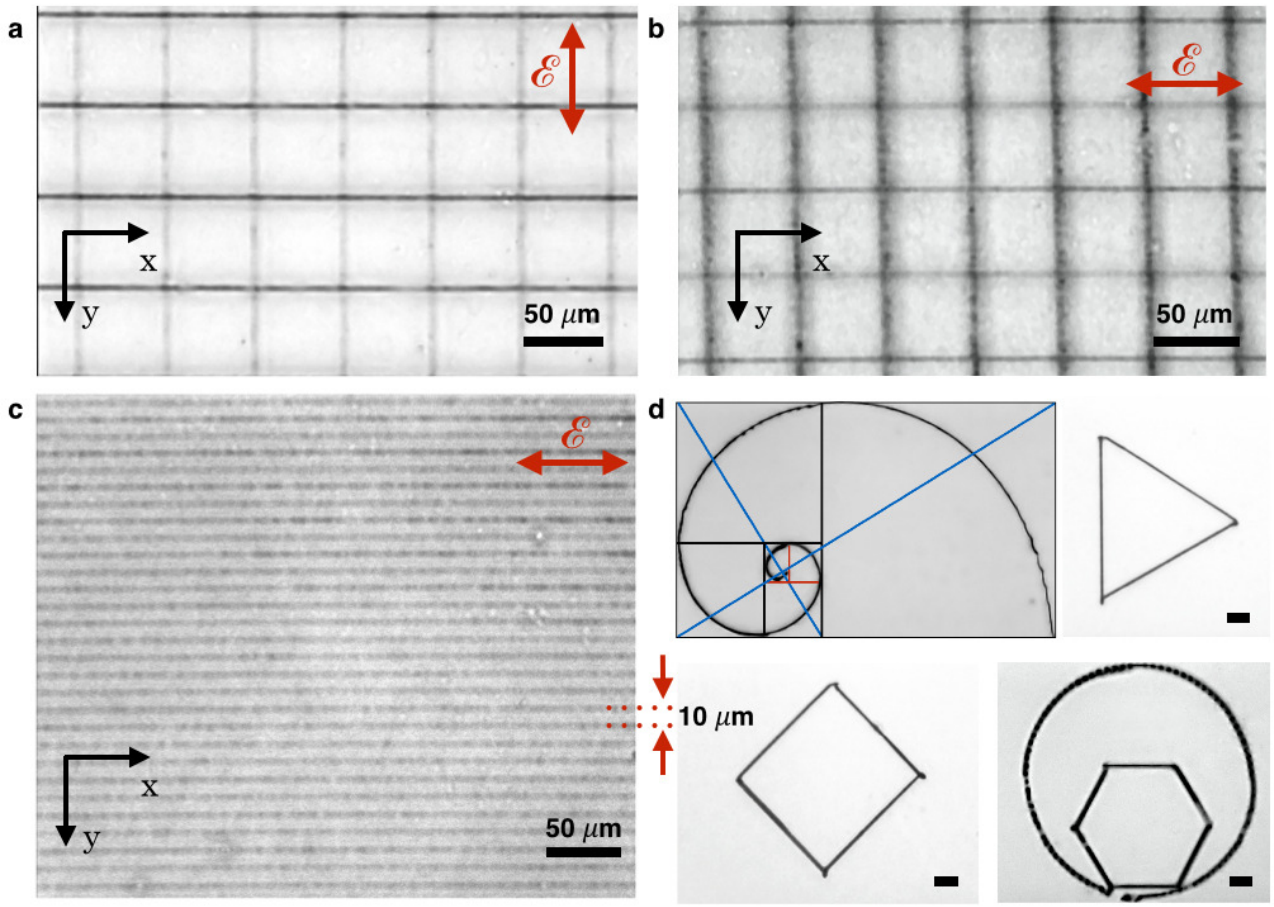

FIG. 3. **Effect of the laser polarization and wall-distance on sub-surface structures.** The polarization (red arrow) is along one of the crystal axes. (***a***) Infrared microscopy images of the subsurface mesh pattern. The sub-surface walls are separated by 50 μm. (***b***) Laser polarization is rotated by 90 degrees (red arrow) and the pattern is repeated. Mesh structure forms with the same laser parameters as in Fig. 3a. Similar quality patterns form irrespective of the scanning direction in both polarizations (See Supplementary Information). The sub-surface walls are separated by 50 μm. (***c***) Closed-packed parallel sub-surface walls. The inter-wall distance is 10 μm. (***d***) Subsurface curved structures written in *n-type* silicon. See Supplementary Figure 1 for n-type and p-type laser-writing parameters and for characterization which is analogous to low doped (150 Ω.cm) silicon scribing.

in Figure 3b. In both Figure 3a and 3b, vertical orientation is written first, and then the horizontal lines are scribed. We observed that the writing order can be switched, i.e., the horizontal lines can be drawn first with either polarization, without any discernible change in

the final pattern. The writing direction did not have any effect on the final structures for both polarizations. In addition,when the angle between the crystal axis and the laser polarization was used as a parameter similar quality structures were produced. This is demonstrated in Figure 3d, by producing subsurface structures in various polygonal geometries, as well as curved shapes such as circles and spirals.

A particularly interesting test would be to see the minimum inter-wall distance one can create. In Figure 3c, we show 10-μm separated walls, drawn with horizontal polarization. It is possible to further push this distance, but we were limited by the resolution of the microscope and the translational stage. However, we could volumetrically write structures in both n-type and p-type silicon and this ability was exploited to create various subsurface shapes and images for the OCT based barcode system described in the following section.

Effect of Doping and Producing Multilayer Structures.

A natural extension of the presented technique is scribing multi-layered buried structures. The preceding experiments were all performed with low doped (p-type, 150 Ω.cm) silicon. Considering the length of the structures along the laser propagation axis ($\approx$ 200 μm) and the wafer thickness (500 μm) one can stack up to two levels on top of each other. To allow for a richer 3D architecture inside the wafer, as well as for controllable chemical etching for 3D microfabrication (which we will elaborate on later), it is highly desirable to have structures with a range of aspect ratios. In particular, shorter lengths along the laser propagation axis are required for multi-layered stacking.

To improve our parameter space, we have performed a complete set of corresponding scribing experiments for n-doped (1 Ω.cm) and p-doped (1 Ω.cm) Si samples (See Supplementary Figure 1). Subsurface walls of similar quality were produced, but with higher threshold pulse energies. For instance, with the same lens (NA=0.55) the threshold pulse energy went from 10 μJ for p-doped (150 Ω.cm) silicon to 15 μJ for both n- and p-doped (1 Ω.cm) silicon samples. The aspect ratios of the structures decreased as well. For p-doped (150 Ω.cm) samples the length of the structure was $\approx$ 200 μm. This value decreased to $\approx$ 180 μm for p-doped (1 Ω.cm) Si and further down to $\approx$ 150 μm for n-doped (1 Ω.cm) Si (Figure 4). The width of the structures remained within a few micron range of 1 μm.

Figure 4 also demonstrates that with the use of an objective and n-doped (1 Ω.cm) silicon,

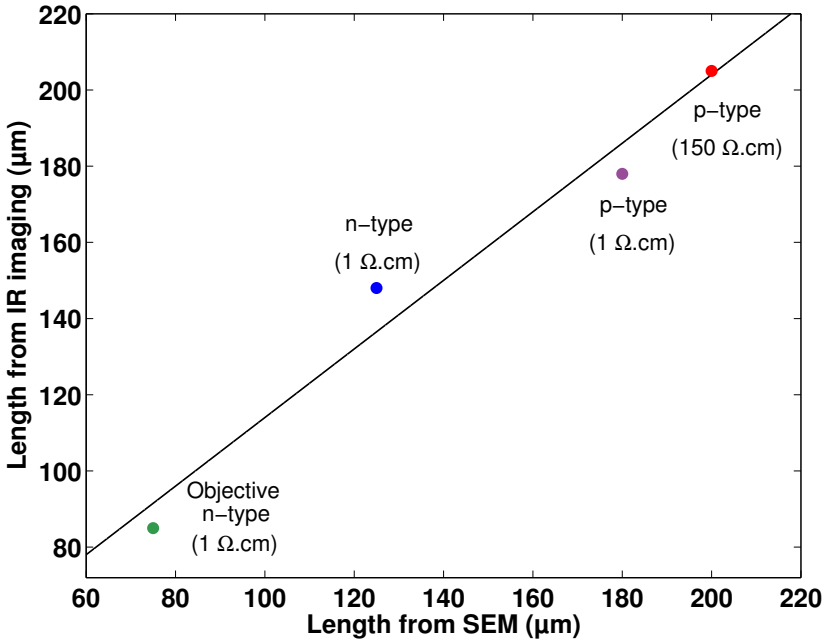

FIG. 4. **Length of the subsurface structures with different scribing methods.** The effect of scribing with a high NA lens and objective is shown. It is observed that increasing doping decrease the structure length along the laser propagation direction. Moreover, the use of an objective further decreases the structure length. A minimum of about 80 μm is attained with the use of an objective.

we can attain about 80 μm long structures. This length-scale enables multi-layered structures embedded in silicon as demonstrated in the next section.

Barcode system with Optical Coherence Tomography Based Readout.

In principle, the presented technique can be used for multi-layered optical data storage applications in silicon. As a proof-of-concept, we first demonstrate two-level structures written in silicon, and later generalize the technique to information encoding in multi-level barcodes with an Optical Coherence Tomography (OCT) based readout.

With the silicon laser-scribing technique we can produce not only continuous walls with various aspect ratios at different doping levels, but also control their positions within the wafer. Figure 5a shows the production method of multi-layered structures, and how their position is manipulated. First, the laser was tightly focused with an objective (NA=1.3) to a depth of 80 μm in n-doped (1 Ω.cm) silicon, and the sample was raster scanned at this depth which produces *Level 1* structures. Then, the focal plane was translated to a depth of

120 μm, and the scan was repeated to produce the structures at *Level 2*. Since production at each depth has a similar threshold pulse energy, it was possible to create the two levels at the same laser parameter set.

The two-level architecture can be visualized with the imaging techniques described previously. For instance, Figure 5b shows the structures of Level 1, while Figure 5d shows the structures of Level 2. Both images were acquired with IR microscopy, therefore the structures at the imaging plane are seen as dark lines, while the other level is visible as a faint shadow. The SEM image directly corresponding to these two images is given in Figure 5c. As also noted in Figure 4, the length of the structures in z-axis is around 80 μm at this operating regime. Therefore, the technique enables optical data encoding in the volume of Silicon wafer. This new 3D architecture suggests the use of a tomographic imaging technology as a readout system for information retrieval without cross-talk between different recorded levels. OCT is the perfect imaging tool for our purposes, since each level can be read individually with a few μm axial and lateral resolution.

In the following, we demonstrate using the inner volume of silicon as an optical data storage medium. We choose the international symbology (Code-128) to encode the information in barcodes. Similar to Figure 5, we write two barcodes at two different levels in silicon. Level 1 encodes "UFOlab", whereas Level 2 encodes "Bilkent". Consecutively, these levels are read from the tomograms generated by the OCT (Figure 6). In the post-processing step, a simple smartphone can be used to decode the barcodes (See Supplementary Movie 2).

Discussion

First we comment on the probable physical origins of the creation of subsurface structures. The observed behaviour is in contrast to the formation of subsurface structures produced with nanosecond lasers in various materials (ref). Formation of these high-aspect ratio structures is analogous to the filamentation effect observed in femtosecond lasers[38]. The tight focusing, along with the doping and thin samples apparently enables us to focus the light in a region where the thermal diffusion results in a narrowly focused heat distribution in the sample. Since the structures are sub-micron in their width, we suggest that a temperature threshold-based mechanism could explain this effect. The repetition rate of the laser is 150 kHz, corresponding to $\approx$ 1.3 nm separation between two laser pulses, therefore we expect

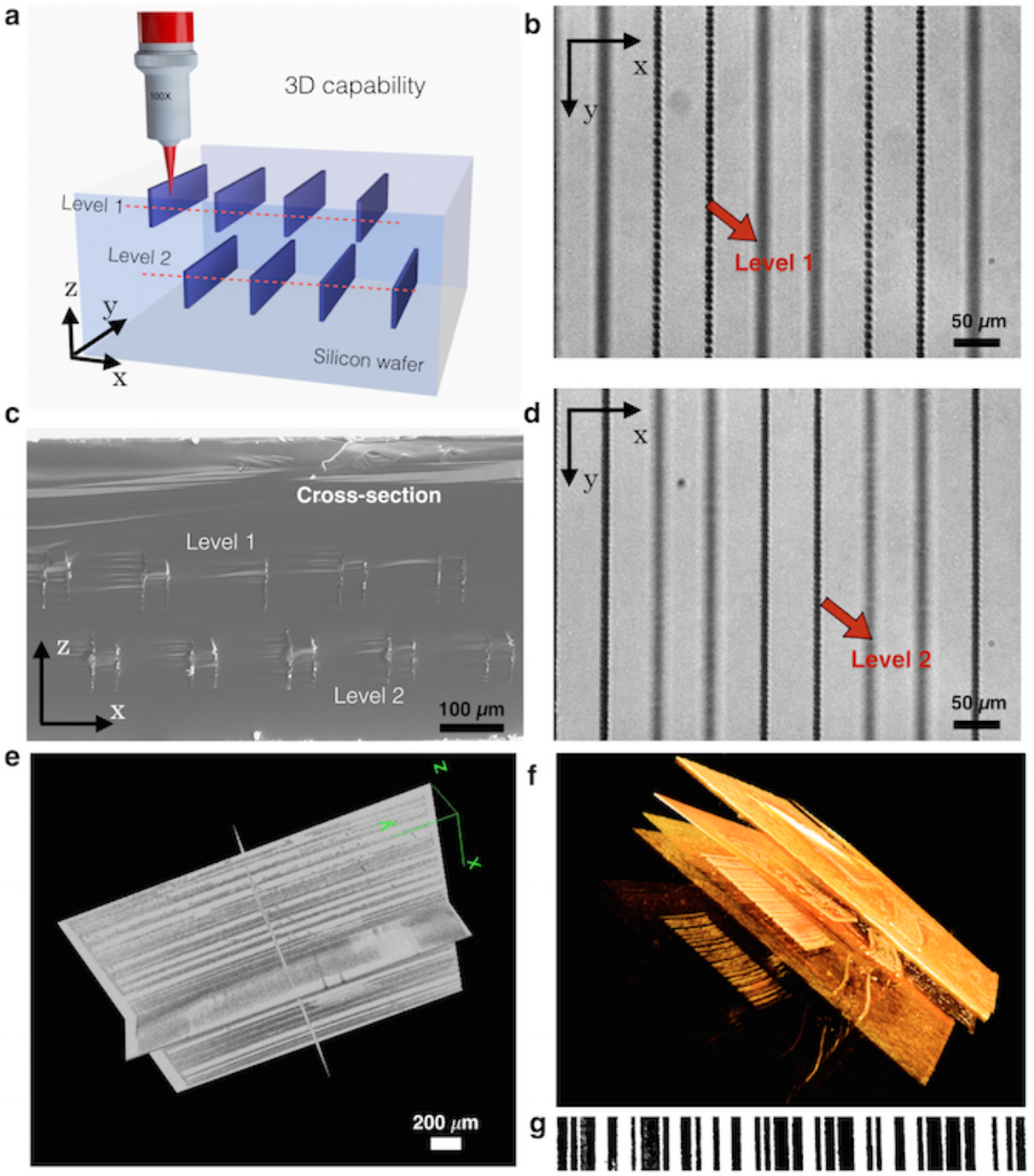

FIG. 5. **Creating multi-level structures in Si.** (***a***) Scheme for silicon laser-scribing for multi-level structures. Tight focusing (NA=1.3, X100 objective) along with optimized pulse energies allow for 3D capability. (***b***) IR image of the plane where the Level 1 structures are formed. The depth is measured to be 230 μm from the laser entrance side. (***c***) SEM image of the cross-section of the processed wafer. At each scribing cycle, two consecutive and adjacent walls are produced at each level. (***d***) IR image of the plane where the Level 2 structures are formed. The depth is measured to be 360 μm from the laser entrance side. ($\boldsymbol{e-f}$) Optical Coherence Tomography (OCT) analysis and tomograms of subsurface structures. (***g***) OCT readout of a buried barcode in Si. One is invited to read the barcode, with a QR code reader, which encodes UFOLab.

a continuous flow of energy to the sample. Since the refractive index of Si is 3.45 at this wavelength, the wavelength inside the sample is 450 nm. Therefore, the heat will mostly be held in a linear geometry, along the propagation direction of the laser before diffusion. If the heat diffusion speed is not fast in the time scale of crystal modification, one may expect a narrow line of laser-writing. However, detailed thermal simulations are required to further elucidate this phenomenon.

Next, we comment on the effect of doping, crystal orientation, laser energy and scanning speed. A coupled set of parameters are laser pulse energy and scanning speed. We observed that there is a threshold energy for the onset of structures, faster or slower scanning speeds can result in "dotted" structures (See Supplementary Figure 3). It is worth noting that both n-doped and p-doped Si can be laser-scribed. Further, we can produce structures at virtually any angle with respect to the crystal angle. It is likely that these two capabilities can be combined on a single wafer, in a rich 3D p-i-n architecture. In particular, one can supplement the already availably lithographic techniques to potentially fabricate optoelectronics elements in 2D and 3D geometries, such as integrated modulators or quantum wells for silicon photonics applications. A particularly exciting application would be creating silicon memories. This requires creating a high number of layers, similar to the previous work done in glass for creating ultra-high density memories.

Since this is a first demonstration of subsurface silicon engineering, there is tremendous room for new studies. On the experimental side, use of tighter focusing can result in different aspect ratio structures. The doping levels of both n-type and p-type silicon can be used as a parameter to further analyse the formation of structures. This is particularly important considering the fact that light interacts with electrons (or holes) in the lattice, which can be tailored by the impurities provided by the doping. Detailed chemical, optical and mechanical studies of the modified areas are required. We may expect photo-induced refractive index changes buried in the wafer. This can be accomplished using femtosecond lasers along with the presented technology. On the theoretical side, 3D finite-element electromagnetic simulations coupled with solutions of thermal diffusion equation are required to shed light on the observed behaviour. We believe the rich parameter space provided by the laser and silicon doping will open new venues in subsurface silicon engineering.

In conclusion, we report the first realization of sub-surface laser modification in Si. This new phenomenon is separated from the previous work in Si, in that the surface is not modified.

In addition, the structures are created in both p-doped and n-doped samples as well as in undoped Si. The buried high-aspect ratio structures have sub-micron widths, which may potentially be used in a range of applications, such as Si dicing, fabrication of Si photonics and solar cells elements. Further, silicon photonics and optoelectronics may significantly benefit from the presented novel fabrication method.

Methods

Experimental setup.

We used optical pulses with a central wavelength of 1550 nm (1.25 eV), a pulse duration of 5.5 ns and a repetition rate of 150 kHz. A schematic of the Er-doped fibre laser system is shown in Supplementary Information Figure XX. The linear polarization angle of the laser was controlled with a half-wave plate, which transforms vertically polarized light to horizontally polarized light. The measurements were performed at room temperature and the approximate laser spot size was ≈ 10 μm on the sample. The laser power was adjusted with a second half-wave plate located between two polarizing beam splitters, operating as an attenuator. Typical laser power before the focusing lens was 1.7 Watts. The laser power was adjusted carefully not to cause any surface damage on the samples. We observed that above 2 Watts before the lens, wafer surface is always damaged. For the p-doped silicon wafers used, approximately % 35 of the energy is reflected from the surface.

After laser-writing, the sub-surface structures were studied by a home-made microscope which uses a broad spectrum LED or halogen lamp as the light source, and an EMCCD camera (Andor^{TM}, Luca S) as the detector. Samples were studied in the transmission mode with a 20X objective (Nikon, 0.45 NA 20X) and a optical filter was used for higher image quality. An optical microscope in the reflection mode (Nikon, 0.6 NA, 40X) is also used to confirm the surface condition before and after the experiments.

Sample preparation and positioning.

Double-side-polished, <100>, p-type silicon samples (Boron doped, 150 Ω.cm) were used in the laser-writing experiments (provided by universitywafer.com). Samples were cut with a diamond-cutter in dimensions of 2 cm x 4 cm to fit on the sample holder, along the crystal

direction. Before usage, the Si samples were than immersed in acid piranha solution for X minutes. Then the samples were cleaned in acetone (5 minutes), ethanol (5 minutes) and deionized water (5 minutes) and later dried with nitrogen flow.

Si samples then were hold in place for processing with Neodymium magnets. For precise sample alignment in the scanning range, interference from the reflections on the two-surfaces of the wafer we utilized. This allowed approximately micrometer level alignment precision throughout the scanning range, and also operated as a proxy for in-situ imaging which significantly assisted during the scans. All scans were performed with a computer controlled, 3-axis translational stage (Thorlabs^{TM}, NanoMax342) at a speed of 0.2 - 1 mm/sec.

REFERENCES

[1]Jalali, B. & Fathpour, S. Silicon photonics. *Journal of Lightwave Technology* **24**, 4600–4615 (2006).

[2]Liang, D., Roelkens, G., Baets, R. & Bowers, J. E. Hybrid integrated platforms for silicon photonics. *Materials* **3**, 1782–1802 (2010).

[3]Kuramochi, E. *et al.* Large-scale integration of wavelength-addressable all-optical memories on a photonic crystal chip. *Nature Photonics* **8**, 474481 (2014).

[4]Lipson, M. Guiding, modulating, and emitting light on silicon - challenges and opportunities. *Journal of Lightwave Technology* **23**, 4222–4238 (2005).

[5]Boyraz, O. & Jalali, B. Demonstration of a silicon raman laser. *Optics Express* **12**, 5269–5273 (2004).

[6]Rong, H. *et al.* An all-silicon raman laser. *Nature* **433**, 292–294 (2005).

[7]Huang, S. M., Sun, Z., Lukyanchuk, B. S., Hong, M. H. & Shi, L. P. Nanobump arrays fabricated by laser irradiation of polystyrene particle layers on silicon. *Applied Physics Letters* **86**, 1619111–161913 (2005).

[8]de Boor, J., Geyer, N., Wittemann, J. V., Gsele, U. & Schmidt, V. Sub-100 nm silicon nanowires by laser interference lithography and metal-assisted etching. *Nanotechnology* **21**, 095302 (2010).

[9]Pedraza, A. J., Fowlkes, J. D. & Lowndes, D. H. Silicon microcolumn arrays grown by nanosecond pulsed-excimer laser irradiation. *Applied Physics Letters* **74**, 2322–2324 (1999).

[10]Tsibidis, G. D., Barberoglou, M., Loukakos, P. A., Stratakis, E. & Fotakis, C. Dynamics of

ripple formation on silicon surfaces by ultrashort laser pulses in subablation conditions. *Physical Review B* **86**, 115316 (2012).

[11]Shen, M. *et al.* High-density regular arrays of nanometer-scale rods formed on silicon surfaces via femtosecond laser irradiation in water. *Nano Letters* **8**, 2087–2091 (2008).

[12]Serpenguzel, A., Kurt, A., Inanc, I., Carey, J. & Mazur, E. Luminescence of black silicon. *Journal of Nanophotonics* **2**, 021770–021770–9 (2008).

[13]Vorobyev, A. Y. & Guo, C. Laser turns silicon superwicking. *Optics Express* **18**, 6455–6460 (2010).

[14]Zywietz, U., Evlyukhin, A. B., Reinhardt, C. & Chichkov, B. N. Laser printing of silicon nanoparticles with resonant optical electric and magnetic responses. *Nature Communications* **5** (2014).

[15]Misawa, H. & Juodkazis, S. (eds.). *3D Laser Microfabrication* (Wiley-VCH Verlag GmbH & Co. KGaA, 2006).

[16]Gattass, R. R. & Mazur, E. Femtosecond laser micromachining in transparent materials. *Nature Photonics* **2**, 219–225 (2008).

[17]Stuart, B. C. *et al.* Nanosecond-to-femtosecond laser-induced breakdown in dielectrics. *Physical Review B* **53**, 1749–1761 (1996).

[18]Carr, C. W., Radousky, H. B., Rubenchik, A. M., Feit, M. D. & Demos, S. G. Localized dynamics during laser-induced damage in optical materials. *Phys. Rev. Lett.* **92**, 87401–1–87401–4 (2004).

[19]Davis, K., Miura, K., Sugimoto, N. & Hirao, K. Writing waveguides in glass with a femtosecond laser. *Optics Letters* **21**, 1729–1731 (1996).

[20]Nasu, Y., Kohtoku, M. & Hibino, Y. Low-loss waveguides written with a femtosecond laser for flexible interconnection in a planar light-wave circuit. *Optics Letters* **30**, 723–725 (2005).

[21]Kowalevicz, A., Sharma, V., Ippen, E., Fujimoto, J. & Minoshima, K. Three-dimensional photonic devices fabricated in glass by use of a femtosecond laser oscillator. *Optics Letters* **30**, 1060–1062 (2005).

[22]Pavlov, I., Dülgergil, E., Ilbey, E. & Ilday, F. O. Diffraction-limited, 10-w, 5-ns, 100-khz, all-fiber laser at 1.55 m. *Opt. Lett.* **39**, 2695–2698 (2014).

[23]Zhang, H., Eaton, S. M. & Herman, P. R. Single-step writing of bragg grating waveguides in fused silica with an externally modulated femtosecond fiber laser. *Opt. Lett.* **32**, 2559–2561

(2007).

[24]Crespi, A. *et al.* Three-dimensional mach-zehnder interferometer in a microfluidic chip for spatially-resolved label-free detection. *Lab Chip* **10**, 1167–1173 (2010).

[25]Crespi, A. *et al.* Integrated photonic quantum gates for polarization qubits. *Nature communications* **2**, 566 (2011).

[26]Marshall, G. D. *et al.* Laser written waveguide photonic quantum circuits. *Opt. Express* **17**, 12546–12554 (2009).

[27]Ttreault, N. *et al.* New route to three-dimensional photonic bandgap materials: Silicon double inversion of polymer templates. *Advanced Materials* **18**, 457–460 (2006).

[28]Gunn, C. Cmos photonics for high-speed interconnects. *Micro, IEEE* **26**, 58–66 (2006).

[29]Carloni, L. P., Pande, P. & Xie, Y. Networks-on-chip in emerging interconnect paradigms: Advantages and challenges. In *Proceedings of the 2009 3rd ACM/IEEE International Symposium on Networks-on-Chip*, 93–102 (IEEE Computer Society, 2009).

[30]Pavlov, I. A., Dulgergil, E., Ilbey, E. & Ilday, F. Ö. 10 w, 10 ns, 50 khz all-fiber laser at 1.55 μm. In *Conference on Lasers and Electro-Optics 2012*, CTu2M.5 (Optical Society of America, 2012). URL `http://www.opticsinfobase.org/abstract.cfm?URI=CLEO_SI-2012-CTu2M.5`.

[31]Kuhn, K. J. Moore's law past 32nm: Future challenges in device scaling. In *Computational Electronics, 2009. IWCE'09. 13th International Workshop on*, 1–6 (IEEE, 2009).

[32]Knechtel, J., Markov, I. L. & Lienig, J. Assembling 2-d blocks into 3-d chips. *Computer-Aided Design of Integrated Circuits and Systems, IEEE Transactions on* **31**, 228–241 (2012).

[33]Fischbach, R., Lienig, J. & Meister, T. From 3d circuit technologies and data structures to interconnect prediction. In *Proceedings of the 11th international workshop on System level interconnect prediction*, 77–84 (ACM, 2009).

[34]Öktem, B. *et al.* Nonlinear laser lithography for indefinitely large-area nanostructuring with femtosecond pulses. *Nature Photonics* **7**, 897–901 (2013).

[35]Leuthold, J., Koos, C. & Freude, W. Nonlinear silicon photonics. *Nature Photonics* **4**, 535–544 (2010).

[36]Mcleod, E. & Arnold, C. B. Subwavelength direct-write nanopatterning using optically trapped microspheres. *Nature nanotechnology* **3**, 413–417 (2008).

[37]Yang, W., Kazansky, P. G. & Svirko, Y. P. Non-reciprocal ultrafast laser writing. *Nature*

Photonics **2**, 99–104 (2008).

[38]Couairon, A. & Mysyrowicz, A. Femtosecond filamentation in transparent media. *Physics Reports* **441**, 47 – 189 (2007).

Acknowledgements

This work was supported by TÜBİTAK under project no. The authors acknowledge useful discussions with .

Additional information

Supplementary information accompanies this paper on http://

Competing financial interests: The authors declare no competing financial interests.

Reprints and permission information is available online at.